DISCLAIMER

This report was prepared as an account of work sponsored by an agency of the United States Government. Neither the United States Government nor any agency thereof, nor any of their employees, makes any warranty, express or implied, or assumes any legal liability or responsibility for the accuracy, completeness, or usefulness of any information, apparatus, product, or process disclosed, or represents that its use would not infringe privately owned rights. Reference herein to any specific commercial product, process, or service by trade name, trademark, manufacturer, or otherwise does not necessarily constitute or imply its endorsement, recommendation, or favoring by the United States Government or any agency thereof. The views and opinions of authors expressed herein do not necessarily state or reflect those of the United States Government or any agency thereof. Reference herein to any social initiative (including but not limited to Diversity, Equity, and Inclusion (DEI); Community Benefits Plans (CBP); Justice 40; etc.) is made by the Author independent of any current requirement by the United States Government and does not constitute or imply endorsement, recommendation, or support by the United States Government or any agency thereof.

Multiscale modeling and laser diagnostics to reveal non-equilibrium reaction chemistry at a plasma-liquid interface

U.S. Department of Energy, Office of Fusion Energy Sciences General Plasma Science (GPS) Program

Grant No. DE-SC0023404

Final Performance Report
September 1st, 2022 – August 31st, 2024

R. Mohan Sankaran (PI) and Davide Curreli (Co-PI)

Department of Nuclear, Plasma, and Radiological Engineering
University of Illinois at Urbana-Champaign
Champaign, IL 61822

Executive Summary

Low-temperature, atmospheric-pressure plasmas in contact with liquid are at the core of a wide range of applications including water treatment, medicine, materials synthesis, and chemical transformation. In general, plasma-liquid processes are scientifically compelling because reactivity can be produced without a catalyst, in relatively inert molecules, such as air or nitrogen and liquid water, in their native states at ambient conditions. However, reactions at a plasma-liquid interface are extremely complex, occurring at a multiphase, gas-liquid boundary where excited or dissociate gaseous species dissolve and react with solution-phase species, and unique reaction pathways are induced by non-equilibrium chemistry. In particular, detailed knowledge of the physical and chemical processes, including what species are produced in the gas phase and how these species are subsequently transported across and react near the interfacial region, remains largely unanswered. In this project, modeling of the non-equilibrium reaction chemistry at the interface of low-temperature, atmospheric-pressure plasmas and liquid water is developed, supported by advanced laser diagnostics.

Research Objective

The objective of this proposed research project is to combine experimental diagnostics and multiphase, multiphysics modeling to provide fundamental insight into the non-equilibrium reaction chemistry and transport at the interface of a low-temperature, atmospheric-pressure plasma and liquid. Specifically, there are two major components to the project activities:

1. Apply laser diagnostics available at the Princeton Collaborative Research Facility (PCRF) to a plasma-liquid process in order to identify and quantify gas-phase radical species that are formed by plasma excitation, dissociation, and reaction of molecular nitrogen (N_2) and water vapor.
2. Develop multiscale modeling to predict the densities of gas-phase species and then assess their permeability and further reaction in the liquid phase.

Details of Accomplishments

The major activities in this project were (i) the design and construction of a gas-phase only plasma reactor at UIUC operated in mixtures of molecular nitrogen (N_2) and water vapor, (ii) one visit to Princeton Plasma Physics Laboratory (PPPL) to use the PCRF and perform laser-induced fluorescence (LIF) and two-photon assisted laser induced fluorescence (TALIF) on the gas-phase humid N_2 plasma, (iii) the design and construction of a plasma-liquid reactor at UIUC with a N_2 plasma in contact with flowing liquid water, (iv) a second visit to PPPL to use the PCRF and perform LIF and TALIF on the N_2 plasma in contact with liquid water, and (v) development of a 0D plasma kinetic model for N_2 and water vapor chemistry. Significant results or key outcomes

and major findings for each of these activities are detailed below.

i. Design and construction of a gas-phase only plasma reactor operated in mixtures of N_2 and water vapor

The focus of our study is plasma-liquid reactors for nitrogen fixation applications. In general, in these reactive system, reactions take place in the gas phase, liquid phase, and in the interfacial plasma-liquid region. While our overall objective is to characterize this system involving a plasma in contact with a liquid, it is complicated because of the multiple phases and practically speaking, challenging to apply optical diagnostics because of the evaporation of the water. For this reason, we designed and set up a model reactor where N_2 and water vapor are introduced in a plasma and there is only a gas phase, as schematically illustrated in **Figure 1a**. An additional advantage of this system is that we can control and vary the water vapor concentration to systematically study the effect of water vapor chemistry. Briefly, the plasma was formed between two pins using direct-current (DC) power. The electrodes were housed in a stainless-steel vacuum chamber to provide control over the background gas. Windows were used to provide optical access for characterization by either optical emission spectroscopy (OES) or LIF. While we operated the plasma at atmospheric pressure with only positive gas flow, the chamber can be pumped as needed, for example to perform calibration of TALIF.

ii. LIF and TALIF measurements on gas-phase humid N_2 plasma at PCRF

An illustration of the principle behind LIF and TALIF is shown in **Figure 1b**. For our applications, LIF is used for molecular species (e.g., NH, OH) and TALIF is used for atomic species (e.g., N, H). In LIF, a single photon excites a target species from a lower energy electronic state to a higher energy electronic state. When the species relaxes, it emits a red-shifted photon. In TALIF, two photons excite the target species simultaneously which is required for higher energy transitions. This three-body collision has a far lower probability of occurring than the two-body collision of LIF; therefore, significantly higher energy lasers must be used for TALIF than LIF. In both cases, excitation and fluorescence occur at precise, albeit broadened, frequencies. With proper calibrations, the fluorescent light can therefore be used to calculate the absolute density of the target species.

In January 2023, we travelled to PPPL to conduct LIF and TALIF measurements at the PCRF on our humid N_2 DC plasma system. After testing the plasma system at UIUC, we brought it to PPPL to ensure the LIF/TALIF measurement were applied on the exact same system, including the stainless steel chamber, electrodes, mass flow controllers (MFCs), humidity control, and the DC power supply. At the PCRF, LIF or TALIF was set up with our chamber as shown in **Figure 1a**. The first task was to align a laser with the plasma to excite target species. While not shown, the laser passes through a series of optical instruments to reshape the beam and focus it. Considering

the plasma is roughly 1-3 mm in length and 1 mm in diameter, this was not a trivial task. Subsequently, the fluorescent emission is captured by a CCD after passing through an optical bandpass filter. An optical filter is required to mitigate capture of light from the plasma itself and from laser reflections in the chamber.

Once these initial tasks were completed and successful measurements of LIF/TALIF were confirmed at a given condition, our goal was to complete a set of measurements over different humidities (i.e., concentrations of water vapor in N_2). To control the humidity, we mixed a flow of dry N_2 and a flow of saturated (100% humidity) N_2, each controlled by a digital MFC. A saturated flow of N_2 was achieved by passing dry N_2 through a water bubbler. The humidity level in the mixed flow was measured by a humidity probe before flowing into the chamber.

It should be noted that the raw LIF/TALIF is only a relative intensity. In order to obtain the absolute species density, which is of interest to us in order to compare with modeling, calibration is required. Briefly, for TALIF, a similar two photon excitation scheme must be used on a gas of known density at both high (atmospheric) and low pressure ($\lesssim$100 torr). For LIF, the signal from Rayleigh scattering must be measured. In both cases, the population of each electronic state (ground and excited) can be modelled by a series of rate equations. Solving the rate equations for TALIF, the density of fluorescing species (not total species density) is expressed in the following form:

$$n_F = n_0 a_{23} \frac{G^2 \sigma^{[2]}}{(h\nu)^2} g(\Delta\nu) \int I_0^2(t) dt$$

where n_F is the density of fluorescing species, n_0 is the ground state density, a_{23} is the branching ratio of the fluorescent transition, G is the amplifier gain, $\sigma^{[2]}$ is the two-photon excitation cross section, $g(\Delta\nu)$ is the overlap integral (a quantity defining the ratio of energy transfer between a laser and spectral line, considering both have finite widths), and I_0 is the laser intensity. This density can then be converted to a detected signal as a function of ground state density. By taking the ratio of the target species signal and a known density signal, we can find the absolute density of the target species:

$$n_N = n_{Kr} \cdot \frac{\eta \sigma_{Kr}^2 a_{Kr} g_{Kr}}{\eta \sigma_N^2 a_N g_N} \frac{(h\nu_N)^2}{(h\nu_{Kr})^2} \frac{S_N}{S_{Kr}}$$

Following the measurements at PPPL, we carried out additional measurements and extensive data processing at UIUC to estimate the species densities. For example, the overlap integral calculation requires the gas temperature of the plasma. OES was performed at UIUC to estimate the gas temperature from the rovibrational lines of N_2. We were also not able to measure some species by LIF such as NH and NO, which we speculated to be because of their near resonant excitation-fluorescence and fast quenching. In this case, OES actinometry was used to measure their densities.

Our final experimental results for the densities of N, H, OH, NH, and NO as a function of relative humidity are shown in **Figure 2**. In general, the density of N is found to decrease with increasing relative humidity, while H, OH, NH, NO increase with relative humidity. These trends are better explained by modeling which is discussed in detail in Section v.

iii. Design and construction of a plasma-liquid reactor with a N_2 plasma in contact with flowing liquid

Following completion of the gas-phase experiments, we developed a plasma-liquid reactor with a flowing liquid surface. A flowing liquid was required to minimize heating which was found to cause condensation on the windows and change the height of the liquid. Both of these effects prevented reliable optical measurements of the plasma. Briefly, the flowing liquid was generated from a liquid reservoir custom-designed and 3D printed to integrate with the existing stainless-steel chamber and ensure the same optical access for diagnostics. Liquid flow was driven by a peristaltic pump to provide stable and pulse-free delivery, and maintain a consistent water level during operation. Figure 3 shows a photo of a DC plasma formed in a pin-to-plane geometry with the flowing liquid surface. A grounded counterelectrode was submerged inside the liquid (not shown). Increasing water flow and gas flow rates was found to minimize heating and completely avoid water condensation and a change in the liquid level.

iv. LIF and TALIF measurements on plasma-liquid reactor

Before performing LIF and TALIF measurements on the plasma-liquid setup, OES was again first used. In addition to verifying the presence of radical species, the measurements were used to estimate the gas and electron temperatures which are needed for the LIF/TALIF analysis. Then the chamber and all supporting equipment, including the new water flow attachment and water pumps, were transported to PPPL in August 2024 for LIF and TALIF measurements at the PCRF. Experiments targeted the detection of N, H, OH, NH, and NH_3 in the gas phase above the liquid interface. The visit was successful as we measured H and OH; however, N, NH, and NH_3 could not be detected despite clear evidence of their optical emission in OES spectra.

Our final density measurements for N, H, OH, NH, and NO as a function of current for both positive and negative polarity are shown in **Figure 4**. Except for OH, a positive polarity plasma was found to produce higher species densities. OH density may not increase because it quickly reacts away due to its fast kinetics as an intermediate species.

The absence of detectable TALIF/LIF signals for N and NH was unexpected since they were observable by OES. We note that LIF and TALIF probe a narrow optical path where the laser intersects a region of the plasma which was in our setup, the positive column, while OES collects

emission from the entire plasma volume at once, including regions of intense electric fields such as the cathode glow. As a result, species concentrated near the electrode regions may contribute strongly to OES spectra but remain below detection limits for LIF/TALIF.

To reconcile these discrepancies, we have recently reconfigured the OES setup to achieve high spatial resolution, enabling spectral collection from distinct regions within the plasma. These spatially resolved OES measurements are now being compared with the LIF/TALIF data to refine our understanding of species distribution and excitation mechanisms near the plasma-liquid interface. Data analysis from these experiments is ongoing.

v. Development of 0D plasma kinetic model for N_2 and water vapor chemistry

The modeling effort was carried out at UIUC. A global chemical-kinetic reaction network was developed for modeling the humid N_2 plasma chemistry consisting of electron-impact reactions, including dissociation, attachment, ionization, recombination, and excitation; thermal reactions, involving heavy neutral particles and ions; and optical transitions. An overview of our overall approach to modeling is outlined in **Figure 5**. Ultimately, we considered a total of 338 reactions and 53 species, including 10 charged species, as summarized in **Table 1**. The reaction network was solved using CRANE, an open-source chemical kinetic solver built on the MOOSE framework, which can be used as a standalone solver. The rate constant or coefficient for each reaction was either calculated or obtained from the literature. For some electron-impact reactions, cross sections from the literature were fed to LoKI-B, an electron Boltzmann equation solver, to calculate rate constants as a function of electron temperature. For other electron-impact reactions and thermal reactions, rate constant expressions as a function of electron temperature and gas temperature were found in the literature.

We performed calculations with inputs from experimental measurements, including the electron temperature, gas temperatures, and relative humidities. **Figure 6a** shows calculation results for the temporal evolutions of a few representative neutral species, N_2, H_2O, N, and H, at two RH values. A steady state was achieved in all cases within a few seconds and the steady-state values were used for further analysis. In achieving a steady state, the densities of the initial reactant species (N_2 and H_2O) decrease with time as expected, reflecting the consumption of N_2 and H_2O to form products. Concomitantly, the densities of product species, including intermediates such as N and H, increase with time. **Figure 6b** shows calculation results for the temporal evolutions of charged species at 90% relative humidity. Again, a steady state was achieved in all cases over a few seconds. In the inset, the total densities of positively-charged and negatively-charged species are shown and found to be equal, confirming quasineutrality. We similarly checked that quasineutrality was achieved at all RH's studied. We note that the predominant negatively-charged species in our network are electrons, as expected, and the predominant positively-charged species

are N_2^+ and N^+. A primary reason that the ionic species are mostly nitrogen is that the background gas is almost entirely made up of N_2 (~97.8 −100% by volume for the range of RH studied).

The global (0D) model outputs the densities of various plasma species spatially averaged over an entire volume. Model calculations were able to reproduce the observed trends and absolute densities obtained by experimental measurements. The main discrepancy was for OH. We note that the 0D model assumes a homogeneous plasma volume, but in actuality, the plasma may not be spatially uniform. In particular, DC glow discharges are characterized by strong and asymmetric electric fields, which will lead to local variations in basic properties such as plasma density and electron temperature, as previously discussed. For example, electrons can be accelerated in the cathode sheath to very high energies, creating a population of hot electrons that deviate from a Maxwellian distribution. Such hot electrons may enhance direct electron impact reactions such as the dissociation of water vapor. The inhomogeneous structure of the plasma may also lead to spatially varying species densities. These changes to the densities would have a particularly large impact on OH, since its density is relatively low compared to other species such as H.

With this validation of the model, we can extend the calculations and analysis to other species to provide further insight into the humid N_2 plasma chemistry. One of the main goals of studying the reactivity between N_2 and H_2O is to develop a sustainable route to nitrogen fixation. The formation of NH_3, perhaps the most important fixed nitrogen product, starts with N and proceeds through NH. The key reaction paths that lead to the formation of NH_3 are illustrated as a process flow schematic in **Figure 7**. Our simulation results show that at low relative humidity, N_2 is initially excited by electrons to either $N_2(A^3)$ or $N_2(v > 0)$, which react further with N_2 or electrons, respectively, to generate N. N subsequently reacts with H to first form NH, and then through sequential H additions forms NH_3. The formation of NH_3 is limited by the reverse reaction of NH to form N, and the relatively low rates for NH to NH_2 and NH_2 to NH_3. As described above, as the relative humidity increases, N decreases and NH is limited despite the increased amount of H from H_2O vapor. There are additional effects of the increase in H. The recombination of H leads to the formation of H_2, which, along with H itself, promotes the continued reactions of NH to NH_2, and NH_2 to NH_3. However, H also is responsible for the reverse reactions of NH_2 to NH and NH_3 to NH_2. The competition between these different pathways can explain the trend we observe for the NH_3 density as a function of relative humidity.

Another important fixed nitrogen product is NO_x (NO and NO_2). As shown in **Figure 7**, our simulation results reveal that N reacts with OH to form NO at low and high relative humidity. This reaction is referred to as the extended Zeldovich mechanism, which is a modified version of the Zeldovich mechanism that describes the formation of NO by reactions between N_2 and O_2 through either N or atomic oxygen (O). The extended Zeldovich mechanism has previously been reported in humid N_2 and humid air. NO can further react to form N_2O and HNO_2 as well. N_2O is formed by the reaction of NO with NH, and HNO_2 is formed by the reaction of NO with OH.

While both H and OH increase in density with increasing relative humidity, as they are by-products of H_2O chemistry, the density of H is much higher than OH across relative humidity. In terms of the rate constants, N is more reactive with H than OH. It is thus surprising that our model calculations show the NO density is substantially higher than that of NH and related species (*i.e.*, NH_2, NH_3). However, in comparing the reactions mechanisms for NH and NO described above and illustrated in **Figure 7**, there are key differences. The reduction pathway involves multiple reaction steps before yielding a stable species, whereas the oxidation pathway only requires one reaction step before a stable species is formed, which makes the latter much more probable. In addition, our analysis revealed that the reverse reactions are comparatively different. In general, the reverse reactions involving NO are found to be less significant than those involving NH by virtue of much lower rate coefficients. For example, if we focus on the formation of NH and NO from N, the rate coefficients of the reverse reactions for NH are orders of magnitude greater than the forward reactions, whereas the rate coefficients of the reverse reactions for NO are orders of magnitude smaller than the forward reactions. We note that reverse reactions for NO are not shown in **Figure 7** because their rates were too low. As a result, the steady-state density of NO is much higher than NH.

Publications (overall)

1. A. Jayanarasimhan, R. Pierrard, S. M. Peyres, S. Yatom, D. Curreli, and R. M. Sankaran, "Insights into sustainable nitrogen fixation by gas-phase spectroscopic measurements and global modeling of reaction intermediates in humid nitrogen plasma," *ACS Sustainable Chem. Eng.* **13**, 140 (2025).
2. R. Pierrard, S. Yatom, D. Curreli, and R. M. Sankaran, "Spatial mapping of radical transport in nitrogen plasma-liquid system via spectroscopic measurements" *In preparation*

Personnel

Ananthanarasimhan Jayanarasimhan – Postdoctoral researcher
Robert Pierrard – Ph.D. expected 2026

Impacts

Our research has revealed fundamental insight into humid N_2 plasma chemistry. To summarize:

1. The generation of N, which is the first step to fixing nitrogen to products such as NH_3, occurs primarily through $N_2(A^3)$ and $N_2(v > 0)$. The lower excitation energy of these

species leads to a higher dissociation rate than direct electron impact dissociation of N_2 to produce N.

2. The density of N exhibits a sudden decrease with increasing RH. In comparison, H increases with increasing RH. Thus, NH does not increase with RH, because generation is limited by N, and consumption is enhanced by (a reaction with) H.
3. The decrease in N with increasing RH is not because of a competing reaction involving N, but rather because a source of N, $N_2(A^3)$, preferentially reacts with a by-product of H_2O activation, H_2. Introduction of H_2O is also not found to quench the plasma as T_e remains relatively constant across RH.
4. The by-products of H_2O activation, H and OH, both react with N, with the former potentially leading to NH_3 and the latter potentially leading to NO_x. Even though the reaction with H has a higher rate, there is a much higher production of NO_x because NH, NH_2, and NH_3 involve multiple steps with kinetically more significant reverse reactions that limit their formation.

The research has involved one postdoctoral researcher and one graduate student. The graduate student is expected to receive his Ph.D. in 2026.

Acknowledgment

This material is based upon work supported by the U.S. Department of Energy, Office of Science, Office of Fusion Energy Sciences under Award No. DE-SC0023034.

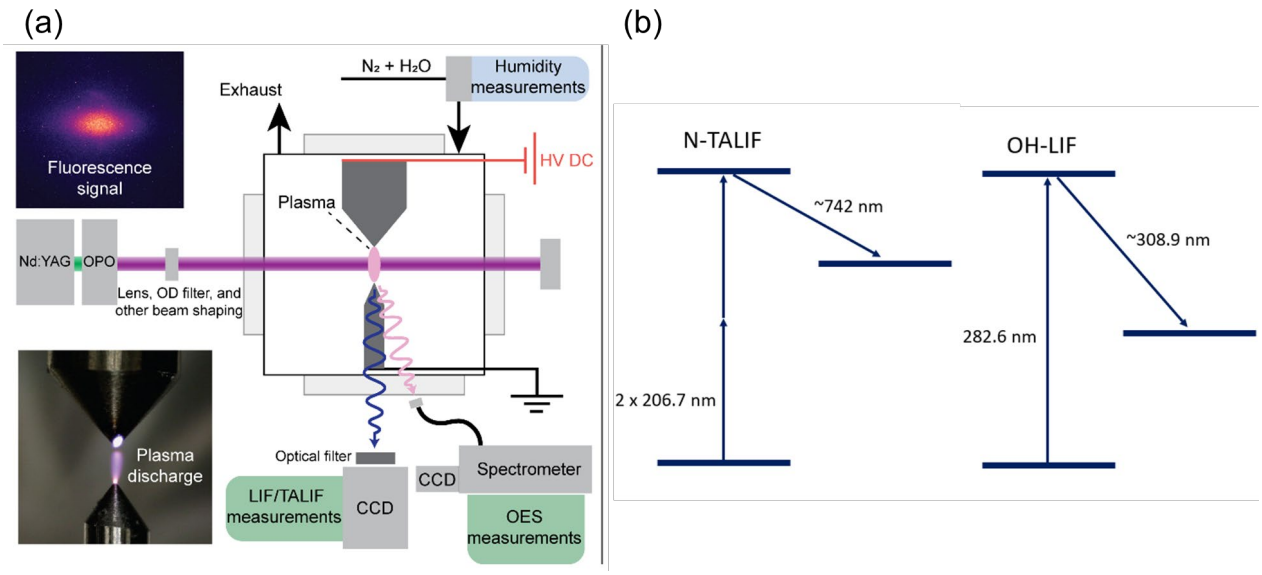

Figure 1. Schematic illustrations of (a) humid N_2, gas-phase plasma reactor that was designed as a model system for optical diagnostics and modeling, and (b) LIF/TALIF excitation and fluorescence processes for N and OH.

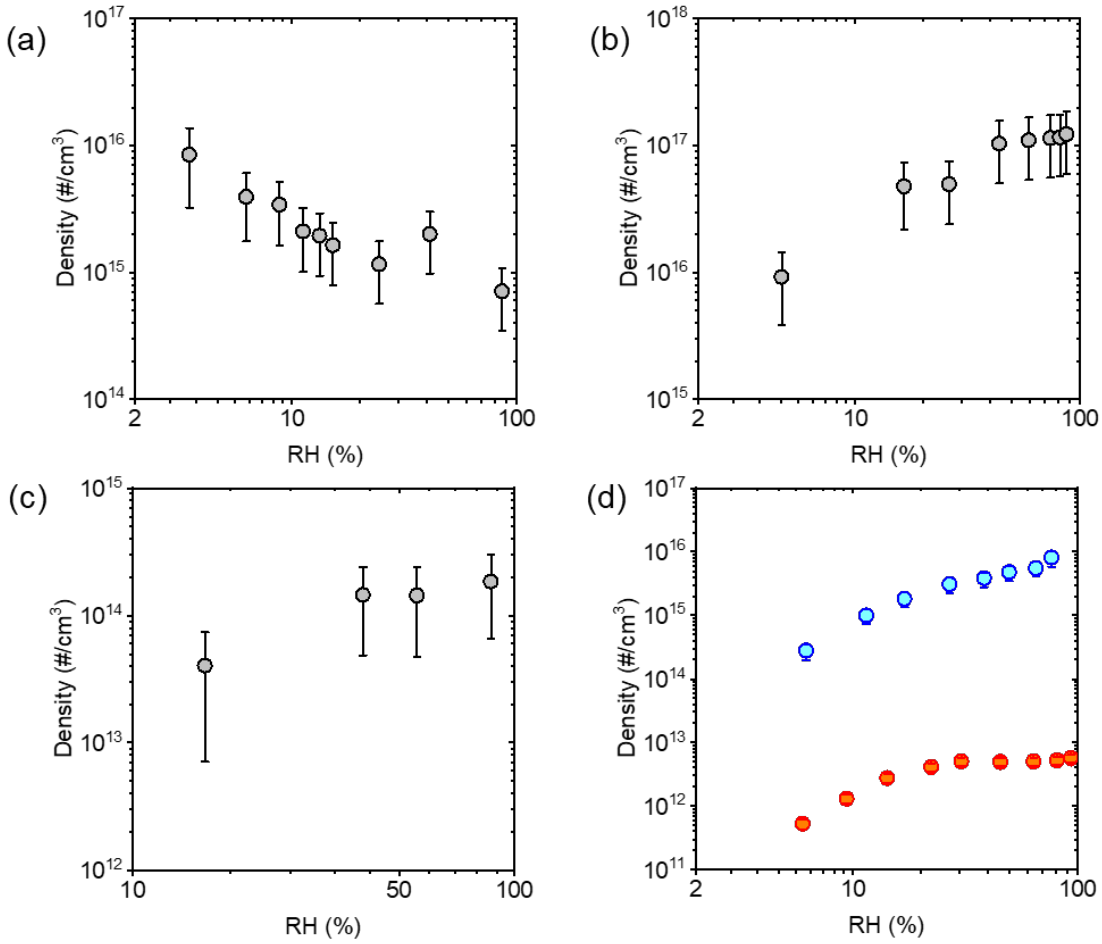

Figure 2. Density as a function of humidity of (a) N, (b) H (c) OH, and (d) NH and NO, experimentally measured by TALIF, TALIF, LIF, and OES, respectively.

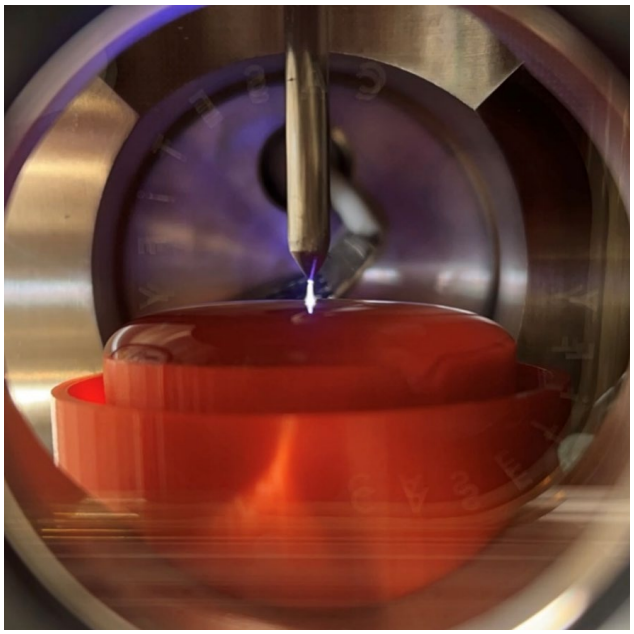

Figure 3. Photo of plasma-liquid reactor operating with a flowing liquid surface in order to avoid heating of the water which leads to condensation on the windows and changes in the liquid level during optical measurements.

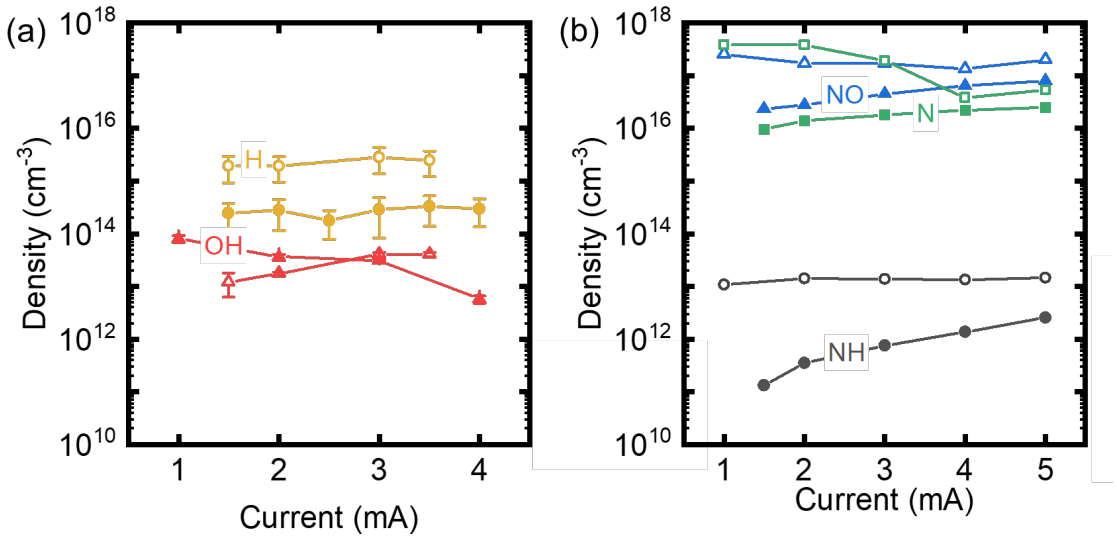

Figure 4. Density as a function of plasma current for (a) H and OH experimentally measured by TALIF and LIF, and (b) N, NH, and NO experimentally measured by OES actinometry. Closed symbols correspond to negative polarity plasma electrode and open symbols correspond to positive polarity plasma electrode.

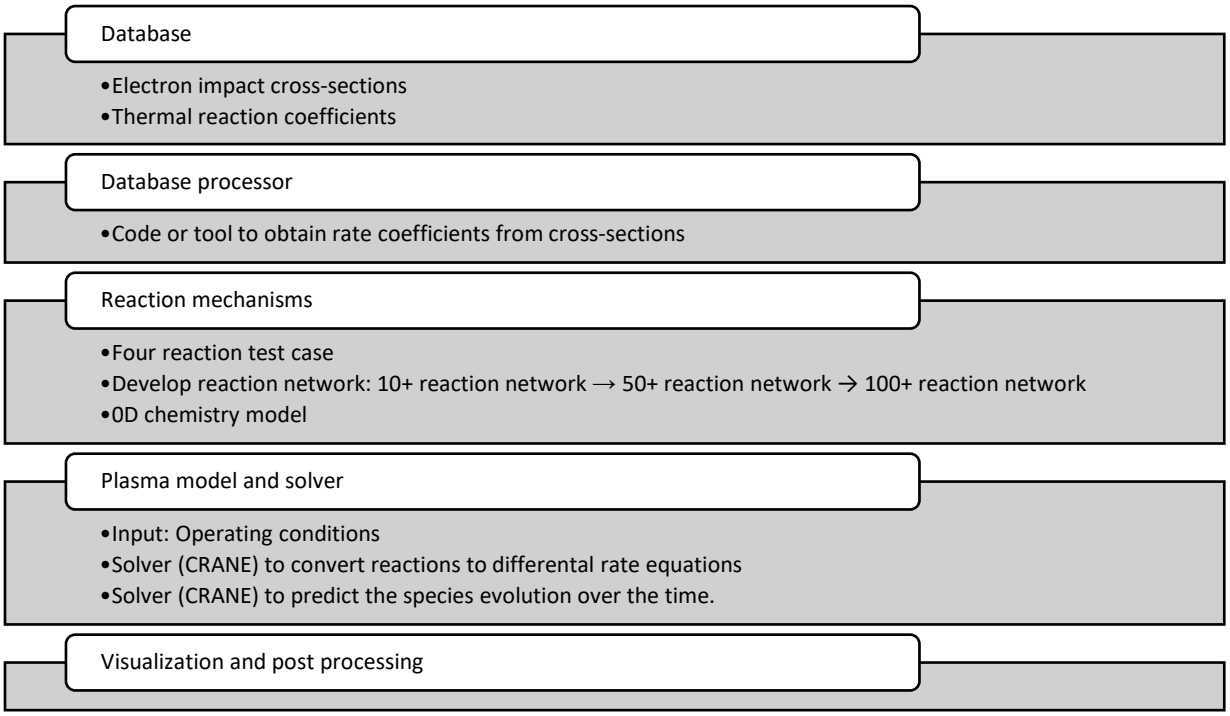

Figure 5. Schematic of process flow for 0D modeling of humid N_2 plasma.

Table 1. Summary of general types of species and reactions considered in the humid N_2 plasma chemical reaction network.

Species type	Details	
Neutrals	N_2, N, NH, NH_2, NH_3, NO, NO_2, NO_3, N_2O, H_2O, OH, HO_2, H_2O_2, O_2, O, O_3, HNO, HNO_2, HNO_3, H_2, H	
Excited neutrals	N_2(v), N_2(A3, B3, C3, a'), H_2O(v), OH(A), O^1D, O^1S, H(n=2,3)	
Charges species	N^+, N_2^+, N_4^+, OH^-, H_2O^+, H_3O^+, O^-, H_2^+, H^+, H^-	
Reaction types	Description of processes	No. of reactions
Electron impact	Excitation/deexcitation, ionization, recombination, dissociation, dissociative attachment/recombination	85
Thermochemistry	Quenching, excitation and ionization of N_2 electronic states	36
	Other neutral-neutral	165
	Ion- neutral reactions	20
	Ion-ion reactions	21
Optical transitions	Radiative decay	11

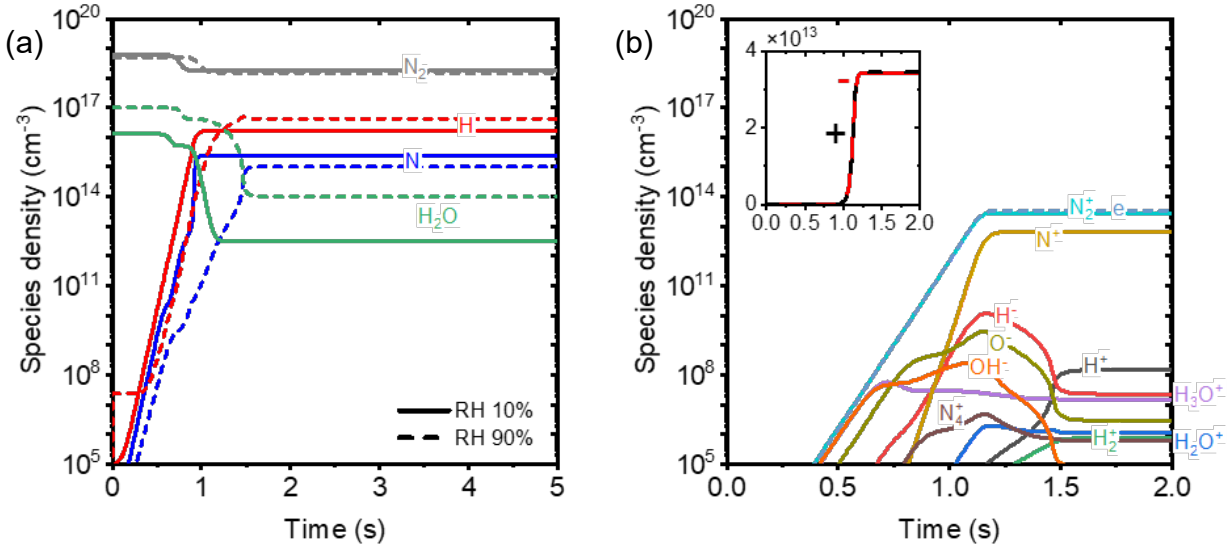

Figure 6. (a) Simulated temporal evolution of N_2, H_2O, N, and H densities at a RH of 10% and 90%. (b) Simulated temporal evolution of charged species densities at a RH of 90%. Inset shows the total density of positive ions (⋯) and negative ions (—), confirming quasineutrality.

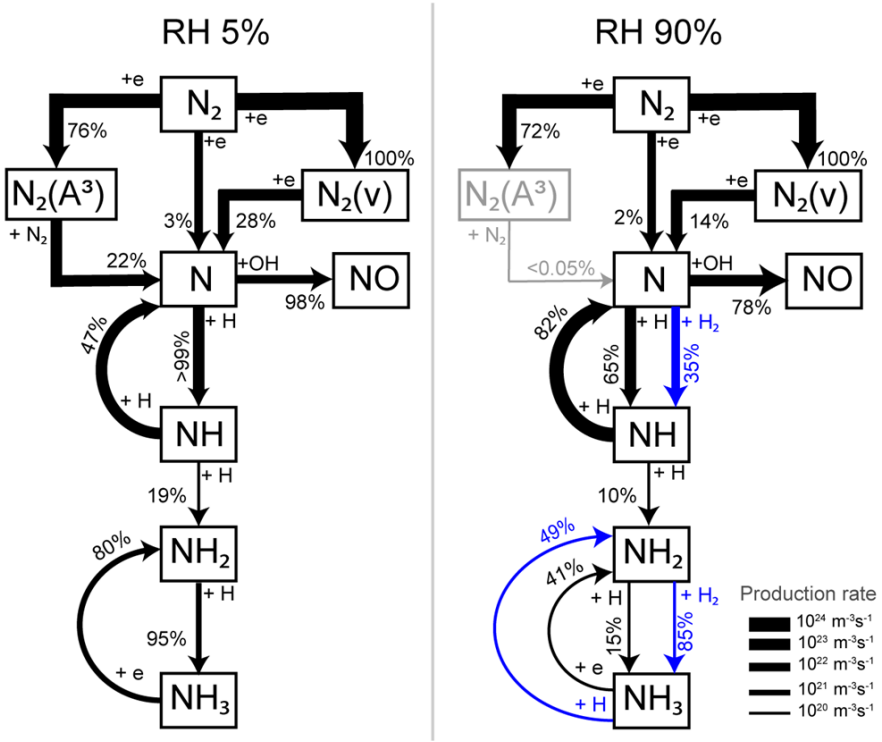

Figure 7. Schematic illustration of mechanisms and reaction pathways for NH_3 and NO production at a RH of 5% and 90%. Blue colored arrows and text indicate reaction channels that are absent at 5%, but opened at 90% RH. Grey colored arrows and text show reaction channels that are active at 5% and deactivated at 90% RH. The thickness of the arrows corresponds to the rate of the reactions specified in the legend. Percent values correspond to the fraction of the species produced from a given reactant. For simplicity, only the dominant reaction channels (1 to 3), summing to >90% of the total production are shown.